

Plasma Sci. Technol. **19** (2017) 055504 (6pp) https://doi.org/10.1088/2058-6272/aa57f5

Influence of the gassing materials on the dielectric properties of air

Hantian ZHANG (张含天)[1], **Tianwei LI** (厉天威)[2], **Bing LUO** (罗兵)[2], **Yi WU** (吴翊)[1], **Fei YANG** (杨飞)[1], **Hao SUN** (孙昊)[1] **and Li TANG** (唐力)[2]

[1] State Key Laboratory of Electrical Insulation and Power Equipment, Xi'an Jiaotong University, Xi'an 710049, People's Republic of China
[2] State Key Laboratory of HVDC, Electric Power Research Institute, China Southern Power Grid, Guangzhou 510080, People's Republic of China

E-mail: sun.hao1031@hotmail.com

Received 18 October 2016, revised 2 December 2016
Accepted for publication 20 December 2016
Published 31 March 2017

Abstract

Influence of the gassing materials, such as PA6, PMMA, and POM on the dielectric properties of air are investigated. In this work, the fundamental electron collision cross section data were carefully selected and validated. Then the species compositions of the air–organic vapor mixtures were calculated based on the Gibbs free energy minimization. Finally, the Townsend ionization coefficient, the Townsend electron attachment coefficient and the critical reduced electric field strength were derived from the calculated electron energy distribution function by solving the Boltzmann transport equation. The calculation results indicated that H_2O with large attachment cross sections has a great impact on the critical reduced electric field strength of the air–organic vapor mixtures. On the other hand, the vaporization of gassing materials can help to increase the dielectric properties of air circuit breakers to some degree.

Keywords: air circuit breaker, gassing materials, Boltzmann equation analysis, dielectric properties, EEDF, critical reduced electric field strength, electron collision cross section

(Some figures may appear in colour only in the online journal)

1. Introduction

Gassing materials, usually polymeric materials, are widely used to improve the interruption performance of electrical switch gears [1] (e.g. the moulded case circuit breaker). An arc with high temperature (greater than a few tens of thousands Kelvin) is generated between the electrodes during the opening process. Gassing materials in the arcing chamber walls are vaporized into organic vapors when exposed to the high-temperature arc plasma.

The detailed mechanisms of why the gassing materials can improve the interruption performance of the circuit breakers have not been well understood. It can be explained from the following three aspects [2]. Firstly, a large amount of hydrogen with favorable heat exchange ability is produced and then can cool the arc effectively. Secondly, the vaporized wall materials will greatly increase the pressure within the arcing chamber. The pressure difference between the arcing chamber and the ambient leads to the strong gas flow which can cool the arc further. Thirdly, the gas flow can then drive the arc into the splitter plates.

A number of investigations have been done on the influence of gassing materials on the dielectric strength of circuit breakers. Most of them focused on the experimental investigation by using different gassing materials. In Shea's work [3], the dielectric breakdown strength between electrodes was investigated using three different arcing chamber wall materials, alumina, polyamide 6/6 (PA6/6) and polyoxymethylene (POM), respectively. It was found that the two thermoplastic materials had better dielectric recovery characteristics than alumina. Tsukima [4] measured the arc voltage and pressure in a model circuit breaker using glass and polymethy methacrylate (PMMA) as wall materials, respectively. It was found that the pressure increase in the PMMA chamber was much higher than that in the glass chamber during both the arc burning and decaying phase.

Some papers contributed to the theoretical study on the effect of gassing materials in air circuit breakers. In Yang's

Table 1. Species in different hot gases.

Name of the gas	The species considered
Air	e−, H, O, N, H_2, O_2, N_2, NO, CO, H_2O, CO_2;
Air/PA6	e−, H, C, O, N, H_2, C_2, O_2, N_2, NO, CH, CO, C_3, H_2O, CO_2, HCN, HNC, CH_3, CH_4, C_2H_2, C_2H_4, C_2H_6, NH_3;
Air/PMMA	e−, H, C, O, N, H_2, C_2, O_2, N_2, NO, CH, CO, C_3, H_2O, CO_2, HCN, HNC, CH_3, CH_4, C_2H_2, C_2H_4, C_2H_6, NH_3;
Air/POM	e−, H, C, O, N, H_2, O_2, N_2, NO, CO, H_2O, CO_2, CH_4, NH_3;

work [1], the influence of three kinds of media: air, 90%air–10%Nylon (PA) and 90%air–10%POM on low-voltage circuit breaker arcs was investigated with a three-dimensional magneto hydrodynamics model. Domejean *et al* [5] used a hydrodynamic model to study the interaction between the arc and the wall materials in a low-voltage circuit breaker. Tanaka [6] calculated the dielectric strengths of hot N_2/O_2 mixtures from 300 to 3500 K based on the Boltzmann equation analysis. Seeger *et al* [7] calculated the critical reduced electric field of synthetic air for high voltage circuit breaker application with consideration of detachment.

However, theoretical analysis of the influence of gassing materials on the dielectric properties in air circuit breakers has not been paid enough attention to. Therefore, the dielectric properties of pure air, air–PA6 ($-C_6H_{11}NO-$), air–PMMA ($-C_5H_8O_2-$) and air–POM ($-CH_2O-$) in different mixing ratios from room temperature to 4000 K are calculated by solving the Boltzmann transport equation in this paper.

In section 2, a description of the mathematical model including the calculation of gas compositions, the selection of electron impact collision cross sections and the calculation of the critical reduced electric field strength, is presented. The computational results, including the ionization, attachment coefficients and the critical reduced electric field strength $(E/N)_{cr}$ (E, the electric field; N, the total number density) under various mixing ratios, temperatures, and pressures, are presented and discussed in section 3. In section 4, the conclusions are drawn.

2. Mathematical model

2.1. Species composition of the hot gas mixtures

The species compositions of air and the air–organic vapor mixtures at different mixing ratios and pressures (0.1–10 atm) from gas temperature to 4000 K were obtained by minimizing the Gibbs free energy [8]. These species compositions were calculated under the assumption of local thermodynamic and chemical equilibrium. The equilibrium composition of the gaseous mixture system at constant temperature T and pressure p minimizes the system's Gibbs energy G:

$$G(T, p, n) = \sum_{i=1}^{w} n_i \mu_i, \tag{1}$$

where $n = \{n_1, n_2, ..., n_w\}$ is the composition of the gaseous mixture, w is the number of species type. The equilibrium composition can then be derived if the chemical potentials $\mu_i = \mu_i(T, p, n)$ are known. Without consideration of species in condensed state, the chemical potentials can be written as [9]:

$$\mu_i(T, p, n) = \mu_i^0(T, p) + RT(\ln p^* + \ln x_i), \tag{2}$$

where $\mu_i^0(T, p)$ is the chemical potential of i in the standard state, R is the gas constant, $p^* = p/p^0$, p^0 is the standard pressure, x_i is the molar fraction of species i.

Due to the complicity of mixed gas compositions, the effect of species with very low mole fraction (10^{-6}) in the temperature range from 300 to 4000 K are ignored for simplicity. The species of different gas mixtures considered in the present calculation are listed in table 1.

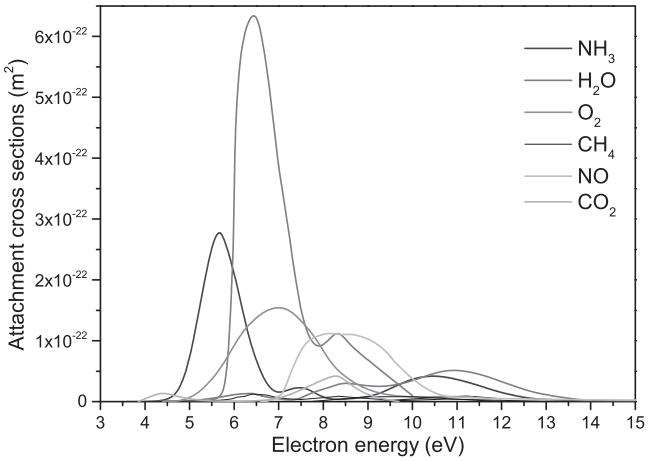

Figure 1. The attachment cross sections of six dominate species.

2.2. Selection of electron collision cross sections

The electron collision cross sections are important fundamental data for the Boltzmann equation analysis. There are lots of electron collision cross section data in different references. However, a large discrepancy exists between different literatures on the electron collision cross sections. Therefore, it is crucial to select and verify the fundamental data before calculation. The electron collision cross section sets of all the calculated species in table 1 are retrieved from the LXC at database [10]. The electron cross sections for H, C, O, N, H_2, N_2, O_2, CO, CH, NO, CO_2, CH_3, NH_3 and CH_4 are derived from Morgan [11], H_2O [12] from Itikawa, C_2, C_3, HCN and CNH from the Quantemol Ltd [13], C_2H_2 [14] and C_2H_6 [15] from Hayashi, C_2H_4 [16] from Puech database.

As the critical breakdown electric fields are obtained when the ionization and attachment coefficients are equal, the ionization and attachment cross sections are crucial to determine the critical breakdown electric field. Figure 1 presents

the attachment cross sections of six dominate species of the air–organic vapor mixtures. It can be clearly seen that H_2O has the largest cross section among all the dominate species. Additionally, the high attachment cross sections of H_2O exist in a broad electron energy range. The attachment cross sections of NH_3, O_2 and NO are smaller than the attachment cross sections of H_2O but higher than that of CO_2 and CH_4.

In the present calculation, the electron momentum transfer cross sections of dominated species like N_2, O, NO and N are much larger than other inelastic cross sections. This allows the calculation of the two-term expansion approximation of the Boltzmann transport equation to obtain the electron energy distribution function (EEDF) [17].

2.3. Solving the Boltzmann transport equation

The EEDF in the air–organic vapor mixtures at applied electric field is calculated by solving the Boltzmann transport equation using the species compositions derived in section 2.1. The BOLSIG+ [18] software (03/2016) is used to solve the Boltzmann transport equation:

$$\frac{\partial n(\varepsilon)}{\partial t} = -\frac{\partial J_f}{\partial \varepsilon} - \frac{\partial J_{\mathrm{el}}}{\partial \varepsilon} + \frac{\partial J_{\mathrm{inel}}}{\partial \varepsilon} + \frac{\partial J_{\mathrm{ion}}}{\partial \varepsilon} + I_{\mathrm{att}} + \left(\frac{\partial n}{\partial t}\right)_{\mathrm{e-e}}, \tag{3}$$

$$n(\varepsilon) = n_{\mathrm{e}} f_0(\varepsilon)\varepsilon^{1/2}; \int_0^{\infty} f_0(\varepsilon)\varepsilon^{1/2}\mathrm{d}\varepsilon = 1, \tag{4}$$

where $n(\varepsilon)\mathrm{d}\varepsilon$ is the electron number density (m^{-3}) in the energy range from ε to $\varepsilon + \mathrm{d}\varepsilon$, $f_0(\varepsilon)$ is the EEDF, J_f, J_{el}, J_{inel} and J_{ion} are the energy gain from acceleration in the electric field, the energy changing rate by elastic collisions with heavy particles, the energy loss by excitation collisions with heavy particle and the energy changing by the ionization collisions, respectively. I_{att} is the energy changing rate by attachment collisions. The collision between electrons is also taken into account in the present calculation by the last term on the right side of equation (3).

At the same time, electron transport coefficients like the Townsend ionization coefficient (α/N) and the Townsend attachment coefficient (η/N) are obtained

$$\frac{\alpha}{N} = \frac{1}{v_{\mathrm{d}}}\sum_{i=1}^{w}\left(\frac{2}{m_{\mathrm{e}}}\right)^{1/2}\int_0^{\infty} x_i\sigma_i^{\mathrm{i}}(\varepsilon)f_0(\varepsilon)\varepsilon\mathrm{d}\varepsilon, \tag{5}$$

$$\frac{\eta}{N} = \frac{1}{v_{\mathrm{d}}}\sum_{i=1}^{w}\left(\frac{2}{m_{\mathrm{e}}}\right)^{1/2}\int_0^{\infty} x_i\sigma_i^{\mathrm{a}}(\varepsilon)f_0(\varepsilon)\varepsilon\mathrm{d}\varepsilon, \tag{6}$$

$$v_{\mathrm{d}} = -\left(\frac{2}{m_{\mathrm{e}}}\right)^{1/2}\left(\frac{eE}{3N}\right)\int_0^{\infty}\frac{1}{\sum_{i=1}^{w}x_i\sigma_i^{\mathrm{m}}(\varepsilon)}\frac{\mathrm{d}f_0}{\mathrm{d}\varepsilon}\varepsilon\mathrm{d}\varepsilon, \tag{7}$$

where m_{e}, e are the mass and charge of electron, σ^{i}, σ^{a}, σ^{m} are the ionization cross sections, the attachment cross sections and the electron momentum transfer cross sections.

The $(E/N)_{\mathrm{cr}}$ is determined when the generation and loss processes of electrons reach a balance [19]. The ionization process causes the generation of electrons while the attachment process leads to the loss of electrons. An electron avalanche could occur when the ionization process is greater than the attachment process (the effective ionization coefficient $\bar{\alpha}/N = (\alpha/N) - (\eta/N)$ is greater than zero). The critical values for electrical breakdown process are obtained when $\bar{\alpha}/N = 0$.

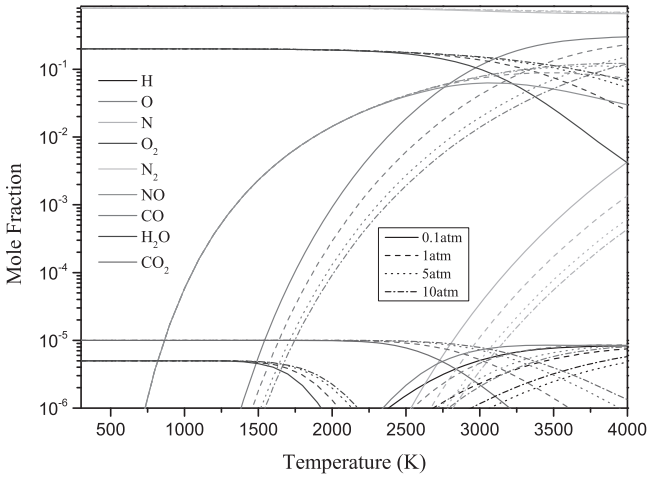

Figure 2. Species composition of pure air as a function of gas temperature at 0.1–10 atm.

3. Results and discussion

3.1. Species composition of the air–organic vapor mixtures

Figure 2 illustrates the calculated composition of pure air as a function of gas temperature at a pressure from 0.1 to 10 atm. In the present calculation, the pure air at room temperature is made up of 79.9998% N_2, 19.9987% O_2, 0.0010% CO_2 and 0.0005% H_2O. At the temperature from 300 to 4000 K, there are mainly neutral particles in air. It can be easily noted that O_2 and CO_2 start to dissociate at about 2200 K. And NO molecules are markedly produced above 1500 K. With the increase of pressure, the dissociations of O_2 and CO_2 can be delayed effectively and the production of NO is inhibited. From figure 2, five species N_2, O_2, NO, O and N are found to be dominated under current condition.

The composition of 95% air: 5% POM and 85% air: 15% POM as a function of temperature at 1 atm are presented in figure 3. Most of the species composition have the same change trends with temperature for two different mixing ratios, except for O_2, which decreases monotonically at 95%:5%, while increases above 2000 K at the mixing ratio of 85%:15%. With the proportion of POM vapor increased in the air–organic gas mixture, the mole fractions of H_2O and H_2 increase greatly. This can be explained by the large amount of H element brought from POM vapor into the gas mixture. On the contrary, the mole fractions of O_2 and NO decrease with more POM adding into the gas mixture.

The composition of several products of 95% air and 5% PMMA gas mixtures with relatively large mole fractions are plotted in figure 4 for comparison at 1–10 atm. With the increase of the gas pressure, the dissociation of H_2O and CO_2 and the generation of O_2 are delayed at the gas temperature above 2500 K. At the temperature lower than 1000 K, CH_4

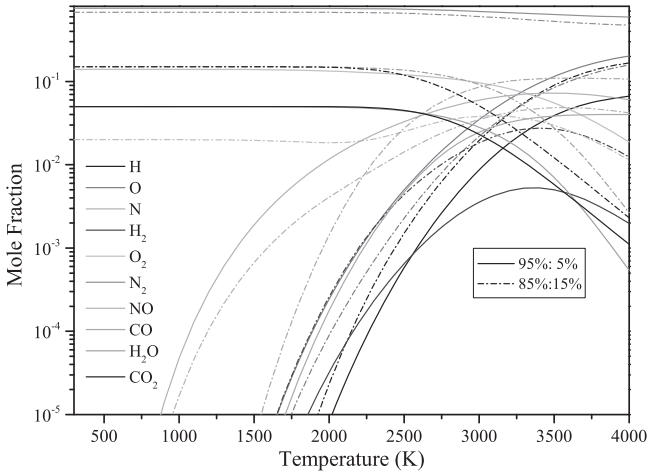

Figure 3. Species composition of air–POM gas mixtures at the mixing ratio of 95%:5% and 85%:15% at 1 atm.

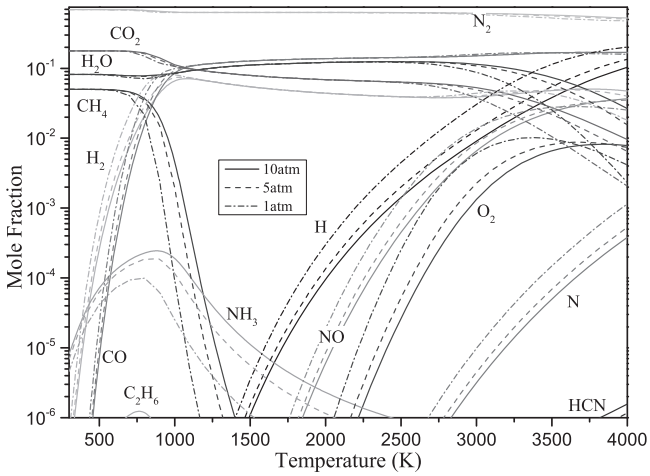

Figure 4. Species composition of 95% air and 5% PMMA gas mixtures at 0.1–10 atm.

cannot be ignored for its relatively large mole fraction. It can be seen that N_2, CO_2, H_2, CO_2 and H_2O become dominated in the temperature range from 1500 to 4000 K. Because of the vaporization of PMMA, the species compositions of 95% air and 5% PMMA gas mixtures are quite different from those of pure air as shown in figure 2. A large amount of H_2 is produced, which is favorable for the heat exchange between the residual hot gas and the ambient gas. On the other hand, H_2O with large attachment cross sections has relatively large mole fraction over the entire temperature range. The generation and decomposition of H_2O will have great influence on the critical reduced electric field strength.

3.2. Comparison of the calculated reduced ionization and attachment coefficients with published data

It is essential to compare the calculated ionization and the attachment coefficients with experimental data from references to confirm the validity of current calculation method and selection of cross sections. Unfortunately, only transport

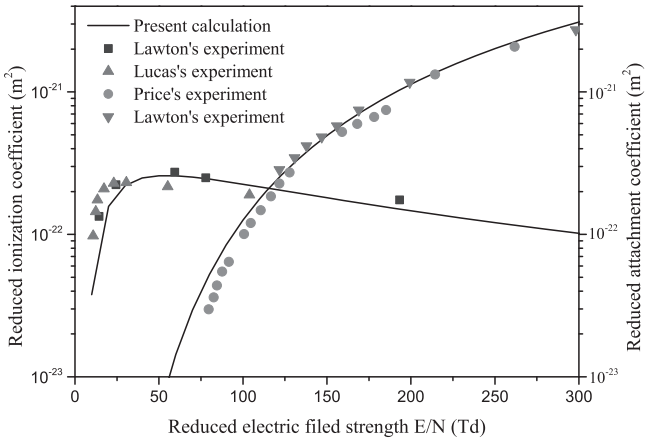

Figure 5. (α/N) and (η/N) of O_2 as a function of E/N at 300 K.

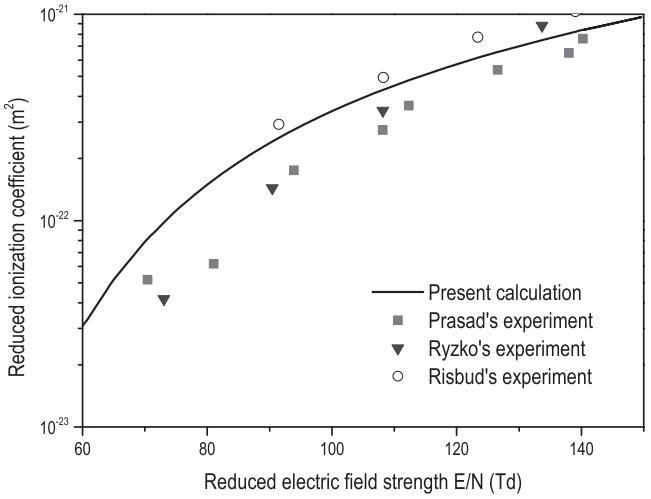

Figure 6. (α/N) of H_2O as a function of E/N at 300 K.

coefficients data for limited kinds of gases are available for now. And most of them were obtained at room temperature.

Figure 5 shows the comparison between the calculated and measured value of the reduced ionization coefficients (α/N) and the reduced attachment coefficients (η/N) of O_2 at 300 K. For the α/N of O_2, the present calculation results are consistent with both Price's [20, 21] and Lawton's [22] work. The result from Price *et al* was suggested by Gallagher [23] to verify the accuracy of calculation for its broad experimental E/N range compared with others. For the α/N of O_2, the present calculation results agree with Lawton's [22] while slightly higher than Lucas's [21] above 50 Td.

Figures 6 and 7 present the reduced ionization and attachment coefficients of H_2O at 300 K with the results from other literatures for comparison [24–27]. Those calculated results agree with the experimental ones.

It can be seen that the cross sections used in the current calculation will lead to the similar results with experiments at room temperature. This validity is essential for the following calculation.

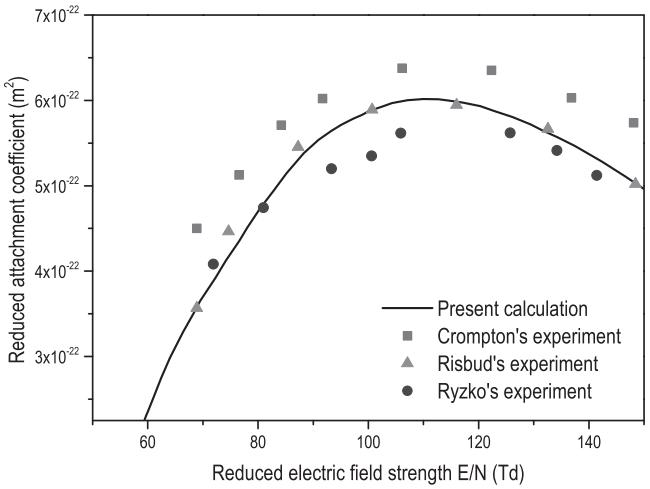

Figure 7. (η/N) of H_2O as a function of E/N at 300 K.

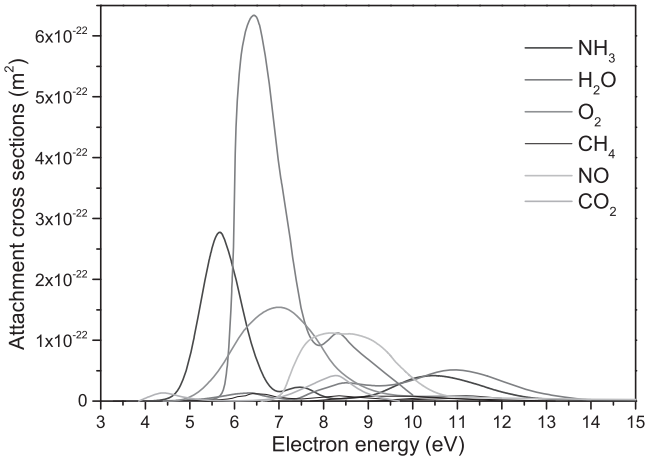

Figure 8. Comparison between $(E/N)_{cr}/(E/N)_{cr0}$ and $(V/\rho)/(V/\rho)_0$ of air.

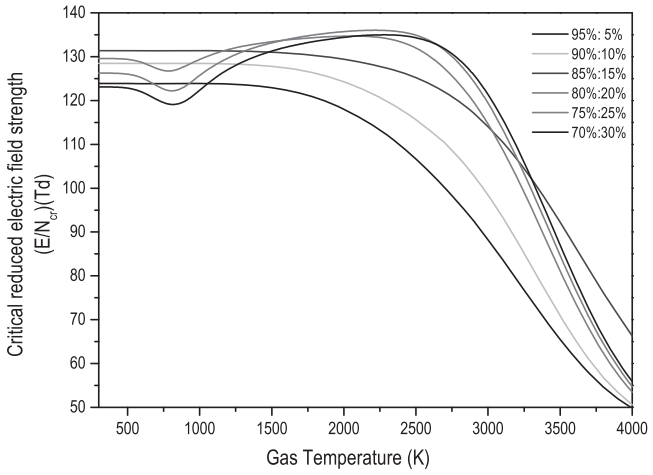

Figure 9. $(E/N)_{cr}$ in air–POM vapor mixture with different mixing ratios at 5 atm.

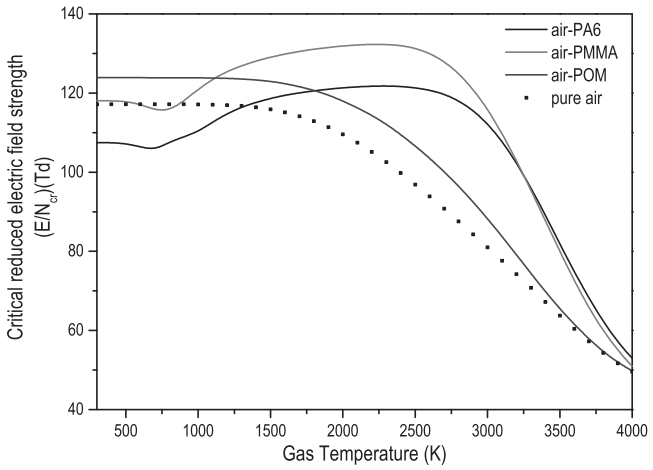

Figure 10. $(E/N)_{cr}$ in different kind of air–organic gas mixtures with the mixing ratio of 95%:5% at 1 atm.

3.3. Critical reduced electric field strength of air and the air–organic vapor mixtures

Rothhardt [28] used a shockwave tube to measure the breakdown voltage of air from 300 to 3500 K. The pressure within the shockwave tube increased from 1 to 5 atm in his experiment. The temperature dependence of the measured reduced breakdown voltage V/ρ (V, the breakdown voltage; ρ, the density) can be approximately equivalent to the $(E/N)_{cr}$ [6]. Figure 8 presents the normalized $(E/N)_{cr}$ (normalized by $(E/N)_{cr}$ at 300 K) and the normalized V/ρ (normalized by V/ρ at 300 K). The temperature dependence of $(E/N)_{cr}/(E/N)_{cr0}$ agrees well with that of $(V/\rho)/(V/\rho)_0$. Therefore, the validity of present calculation method can be confirmed.

Figure 9 shows the critical reduced electric field strength in the air–POM vapor mixture with different mixing ratios at 5 atm. When the mixing ratio is higher than 85%:15%, the $(E/N)_{cr}$ decreases monotonically with gas temperature and the $(E/N)_{cr}$ increases with more POM vapor added into the gas mixture. This phenomenon can be explained as follows: as shown in figure 3, the vaporization of gassing materials brings in the air–POM vapor mixture with plenty of H element, then H_2O with large attachment cross sections is generated leading to higher attachment coefficients of the gas mixture. Keeping increasing the mole fraction of POM vapors, there is an obvious valley of $(E/N)_{cr}$ at the gas temperature around 1000 K. Then the $(E/N)_{cr}$ reaches its maximum at 2700 K. The reason for the $(E/N)_{cr}$ valley at low temperature is the extremum of the mole fraction of H_2O at low air–POM vapor mixing ratios.

Figure 10 presents the critical reduced electric field strength of pure air, air–PA6, air–PMMA, air–POM vapor mixtures as a function of gas temperature at the mixing ratio of 95%:5% at 1 atm. The $(E/N)_{cr}$ of air/POM and pure air changes consistently with temperature. While for air–PMMA and air–PA6, the $(E/N)_{cr}$ experience slight growth from about 800–3000 K and sharp decrease above 3000 K. The slight increase of the $(E/N)_{cr}$ is mainly because of the generation of CO. As shown in figures 3 and 4, the mole fraction of CO increase with temperature, mainly because of the dissociation of CO_2. CO has larger vibration cross sections than other species and the electron energy will be effectively reduced due to the vibration excitation reactions, which is also reported by Stoller [29]. Additionally, vaporizing the same

moles of PA6, PMMA and POM, the ratio of C element produced is 6:5:1. This can be the reason why the $(E/N)_{cr}$ of air–POM mixture as a function of gas temperature is not quite similar to the other two gas mixtures. Around 3000 K, the $(E/N)_{cr}$ begins to decrease due to the dissociation of H_2O and O_2. As can be seen from figure 10, the $(E/N)_{cr}$ in air based organic vapor mixtures are higher than that in pure air from 1500 to 3500 K. The vaporization of gassing materials can enhance the dielectric properties in some degree.

However, it must be noticed that a relatively high value of $(E/N)_{cr}$ in air–PMMA vapor mixture in figure 10 does not necessarily mean that PMMA is the best choice among these three gassing materials to improve the dielectric property of air circuit breakers during arc decay. The cooling effect of vaporized gassing materials cannot be taken into consideration in the present calculation, which has a non-negligible influence on the dielectric property.

4. Conclusion

The critical reduced electric field strength of air and air based organic vapor mixtures (air–PA6, air–PMMA and air–POM) from 300 K to 4000 K were investigated by solving the Boltzmann transport equation. The compositions of hot mixture gases were obtained by the minimization of Gibbs free energy. 23 species (including the electron) were selected for the calculation of air–PA6 and air–PMMA and 14 species (including the electron) for air–POM.

The point that the fundamental electron collision cross section data for this calculation should be carefully selected and validated was stressed in this paper. The cross sections used were validated by comparison between the published literatures and calculation results in the present calculation. The calculation results indicate that the species composition of the air–organic gas mixtures can be quite different from that of pure air. And H_2O with large attachment cross sections has a great impact on the $(E/N)_{cr}$. The $(E/N)_{cr}$ of different air–organic gas mixtures show that the vaporization of gassing materials can be helpful to increase the critical reduced electric field strength in some degree, which verifies the validity of using gassing materials to improve the dielectric properties in air circuit breakers from a theoretical point of view. However, it has be noted that the current interruption performance of practical circuit breaker is a complex process and should not be determined only by the $(E/N)_{cr}$ during the current-zero period. Further work should be focused on coupling the simulation of arc behavior and the calculation of the $(E/N)_{cr}$ to predict the probability of the dielectric breakdown in circuit breakers.

Acknowledgments

This work was supported by the National Key Basic Research Program of China (973 Program) 2015CB251002, National Natural Science Foundation of China under Grant 51521065, 51577145, the Fundamental Research Funds for the Central Universities, and Shaanxi Province Natural Science Foundation 2013JM-7010.

References

[1] Qian Y *et al* 2006 *Plasma Sci. Technol.* **8** 680
[2] Chen D G, Li Z P and Liu H W 2004 *IEICE Trans. Electron.* **87** 1336
[3] Shea J J 2001 *IEEE Trans. Compon. Packag. Technol.* **24** 342
[4] Tsukima M *et al* 2002 *IEEJ Trans. Power Energy* **122** 969
[5] Doméjean E *et al* 1997 *J. Phys. D: Appl. Phys.* **30** 2132
[6] Tanaka Y 2004 *J. Phys. D: Appl. Phys.* **37** 851
[7] Seeger M *et al* 2005 *J. Phys. D: Appl. Phys.* **38** 1795
[8] Wang W Z *et al* 2012 *Phys. Plasmas* **19** 083506
[9] Coufal O, Sezemský P and Živný O 2005 *J. Phys. D: Appl. Phys.* **38** 1265
[10] Girard R *et al* 1999 *J. Phys. D: Appl. Phys.* **32** 2890
[11] Morgan database, www.lxcat.net, retrieved on 17 April 2016
[12] Itikawa Y 2005 *J. Phys. Chem. Ref. Data* **34** 1
[13] QUANTEMOL database, www.lxcat.net, retrieved on 17 April 2016
[14] Capitelli M and Bardsley J N 1990 *Nonequilibrium Processes in Partially Ionized Gases* (New York: Plenum)
[15] Pitchford L C *et al* 1987 *Swarm Studies and Inelastic Electron–Molecule Collisions* (New York: Springer)
[16] Fresnet F *et al* 2002 *J. Phys. D: Appl. Phys.* **35** 882
[17] Tanaka Y 2005 *IEEE Trans. Dielectr. Electric. Insul.* **12** 504
[18] Hagelaar G J M and Pitchford L C 2005 *Plasma Sources Sci. Technol.* **14** 722
[19] Sun H *et al* 2016 *Plasma Sci. Technol.* **18** 217
[20] Price D A, Lucas J and Moruzzi J L 1972 *J. Phys. D: Appl. Phys.* **5** 1249
[21] Lucas J, Price D A and Moruzzi J L 1973 *J. Phys. D: Appl. Phys.* **6** 1503
[22] Lawton S A and Phelps A V 1978 *J. Chem. Phys.* **69** 1055
[23] Gallagher J W *et al* 1983 *J. Phys. Chem. Ref. Data* **12** 109
[24] Prasad A N and Craggs J D 1960 *Proc. Phys. Soc.* **76** 223
[25] Ryzko H 1965 *Proc. Phys. Soc.* **85** 1283
[26] Risbud A V and Naidu M S 1979 *J. Phys. Colloques* **40** C7–77
[27] Crompton R W, Rees J A and Jory R L 1965 *Aust. J. Phys.* **18** 541
[28] Rothardt L *et al* 1981 *J. Phys. D: Appl. Phys.* **14** 715
[29] Stoller P C *et al* 2013 *IEEE Trans. Plasma Sci.* **41** 2359